An Improved Design of Quasi-Optical
Mode Conversion of Whispering Gallery
Mode Gyrotron Radiation

Möbius, A.W.[†], Casey, J.A., Kreischer, K.E.

Li, A., and Temkin, R.J.

Plasma Fusion Center

Massachusetts Institute of Technology

Cambridge, MA 02139

April 1990

[†] Present Address: Kernforschungszenstrum Karlsruhe, Institut für Technische Physik, Karlsruhe, West Germany.

Abstract

Results are reported of a theoretical and experimental investigation of a quasi–optical mode converter for the transformation of whispering gallery mode gyrotron output into a Gaussian like beam. The mode converter consists of a helically cut waveguide launcher, similar to that originally proposed by Vlasov *et al*, followed by a focusing mirror. Theoretical results using aperture field methods indicate that the length of the waveguide launcher is of critical importance in providing a confined radiation pattern. Experimental results on the radiation pattern were obtained for several launcher lengths using a 0.6 MW, 149 GHz pulsed gyrotron operating in the $TE_{16,2}$ mode. Radiation pattern results for the best launcher length agree well with theoretical calculations using the Stratton–Chu aperture radiation theory for unperturbed waveguide modes. A mirror focusing in the azimuthal direction was designed by a geometrical optics approach to focus the radiation coming from the launcher. Good focusing with 91.4% efficiency (power in the focused beam divided by gyrotron power) was found experimentally using the combined launcher and mirror with the pulsed gyrotron. These results indicate that quasi–optical antennas are useful for transforming high order, high frequency gyrotron modes into directed beams in free space.

Introduction

It is desired to convert electromagnetic waves produced by over-moded gyrotrons to low–order mode, linearly polarized waves (for plasma heating via transmission in a corrugated waveguide using the HE_{11} mode[1] or free space Gaussian beam propagation). The typical output modes, TE_{mp}, for high power gyrotrons, have a large azimuthal index (m) and small radial index (p); the so called whispering gallery modes (WGM).

Mode conversion to low–order linearly polarized radiation must meet two requirements. First, the rather complex polarization must be "unwound" into a linear polarization for efficient plasma heating. Second, the highly structured waveguide fields must be efficiently transformed into a low order mode suitable for transmission. The radiation emanating from a circular aperture (or truncated waveguide) is unsuitable for long path transmission or plasma heating, since a WGM gyrotron has the radiation pattern of a hollow cone (with $2m$ azimuthal lobes for non–rotating modes).

The goal of this research program is the efficient conversion of rotating TE_{mp} whispering gallery modes into narrow beam waves. To design a mode conversion system, we start with the quasi–optical configuration, known as a Vlasov converter[2]. It consists of a waveguide opening which serves as a launcher bounded by a straight axial cut and a helical cut, combined with a parabolic reflector, as shown in Fig. 1. (In our terminology, the launcher refers only to the waveguide aperture, while the converter refers to the launcher and mirror system.) The radiation spills from the axial cut, and is directed in a beam with a fixed polar angle and a moderate azimuthal angle spread. The reflector focuses in the azimuthal direction. The original quasi–optical converter design treated TE_{mp} modes for $p = 1$, where an assumption of a line source close to the launcher edge is allowed. We explicitly treat $p > 1$, where the radiation source is distributed inwards from the waveguide wall.

Alternate methods for dealing with the distributed source difficulties for $p > 1$ include converting the operating mode down to $TE_{m,1}$ via radial perturbation mode converters[3], or partially converting to $TE_{m,p+1}$ and $TE_{m,p-1}$ to suppress sidelobe formation[4]. These methods will not be treated here since they are not applicable for use in a
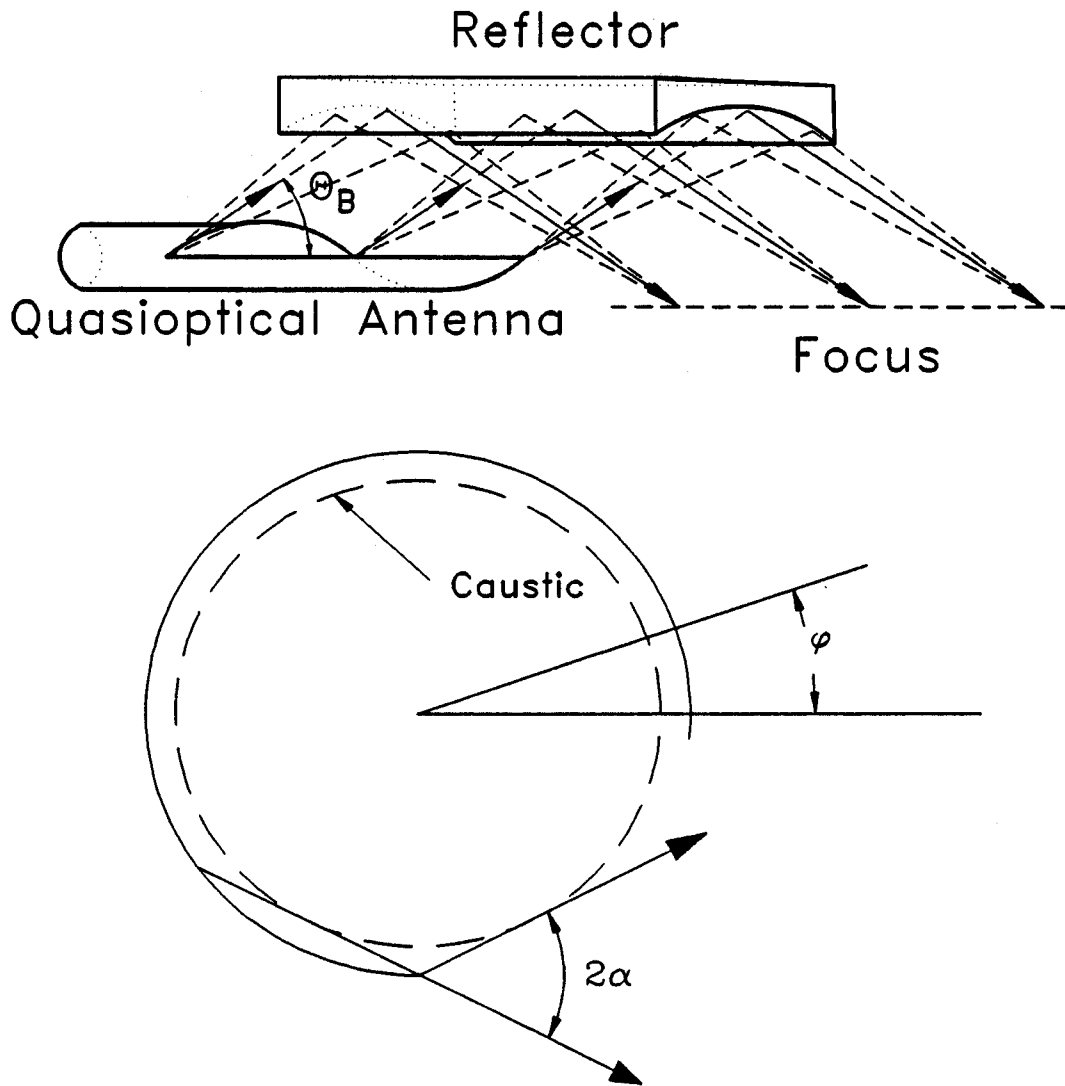
3

Figure 1.   *a.)* The mode converter configuration is shown in perspective, with the helically cut launcher, radiation at the polar angle (θ_B), (the bounce angle), and the two-dimensional focus reflector. The reflector as shown focuses the azimuthal spread in the launcher radiation pattern to a line focus. *b.)* The cross section of the waveguide shows the caustic radius, the extreme azimuthal angles of the radiation pattern, limited by $\cos \alpha = m/\nu_{mp}$, and the azimuthal angle coordinate definition. The launcher edge is at an angle $\phi = -\pi/2$, and the radiation is centered around $\phi = 0$.

4

step tunable gyrotron.

In this research we have derived a general theory to describe the radiation from such a launcher. We also have improved the parameters of the helical launcher and reflector over previous experiments[2,5,6], and verified the converter performance experimentally on a MW gyrotron hot test for TE_{mp} modes with $p = 2$.

Rotating and Counter–Rotating Modes

The helical cut of the Vlasov launcher fixes the mode converter applicability to either right or left handed rotating modes. In our experiments, the gyrotron interaction is destabilized at either one rotation or the other exclusively, depending on the radial position of the electron beam and the corresponding sign of the coupling coefficient[7,8]. In practice, a single converter could be incorporated into a sealed gyrotron tube, and used in either parameter range by reversing the polarity of the magnetic fields at the cavity and electron gun.

Properties of Rotating Modes

The TE waveguide fields generated by a WGM gyrotron can be written in cylindrical coordinates as:

$$\mathbf{H} = H_0\, e^{i(k_z z \pm m\phi - \omega t)}\, \left[\frac{i k_z}{k_r} J'_m(k_r r)\hat{r}\; \mp\; \frac{m k_z}{k_r^2 r}\, J_m(k_r r)\hat{\phi}\; +\; J_m(k_r r)\hat{z} \right] \tag{1}$$

$$\mathbf{E} = Z_0 H_0\, e^{i(k_z z \pm m\phi - \omega t)}\, \left[\mp \frac{m k_f}{k_r^2 r} J_m(k_r r)\hat{r}\; -\; \frac{i k_f}{k_r} J'_m(k_r r)\hat{\phi} \right], \tag{2}$$

for propagation in the $+\hat{z}$ direction, where $\pm$ terms refer to right–handed $(+)$ and left–handed $(-)$ azimuthal rotation. Here, k_f is the free space wavelength, k_r is defined by $k_r \equiv \nu_{mp}/R_w$ where ν_{mp} is the pth zero of $J'_m(x)$ and R_w is the waveguide radius, k_z is the guide wavelength defined by $k_z^2 \equiv k_f^2 - k_r^2$, and Z_0 is the free space impedance given by $\sqrt{\mu_0/\epsilon_0}$. One feature of rotating whispering gallery modes is that the time averaged Poynting vector shows a real azimuthal component of energy flux.

These fields can be represented as superpositions of plane waves by decomposition of the Bessel functions in $\mathbf{E}$. This is quite useful in

approximating the design of reflector surfaces in the near field. The result of this decomposition yields[9] (for right hand rotation):

$$E_r = -\int_0^{2\pi} d\phi' \, E_0 \cos\phi' \, e^{i(-\omega t + k_z z + k_r r \sin\phi' + m(\phi-\phi'))}, \qquad (3)$$

$$\text{and} \quad E_\phi = \int_0^{2\pi} d\phi' \, E_0 \sin\phi' \, e^{i(-\omega t + k_z z + k_r r \sin\phi' + m(\phi-\phi'))}, \qquad (4)$$

given that

$$E_0 \equiv H_0 \frac{Z_0 k_f}{2\pi k_r}. \qquad (5)$$

In this expansion, the fields are represented by a continuum of plane waves according to the form

$$E_{\phi'} \propto e^{i(k_f S(\mathbf{r}) - \omega t)} \qquad (6)$$

where the eikonal $S(\mathbf{r})$ is given by

$$k_f S(\mathbf{r}) \equiv k_z z + k_r r \sin\phi' + m(\phi - \phi'). \qquad (7)$$

Solving the eikonal equation

$$(\nabla S)^2 = 1 \qquad (8)$$

yields an intuitive picture of the propagation paths of these plane waves, or rays[10]. We see that

$$\phi'(r = R_w) = \alpha, \qquad \cos\alpha \equiv \frac{m}{\nu_{mp}}, \qquad (9)$$

where α is the azimuthal bounce angle of the rays between the guide surface and a tangent plane to the guide (see Fig. 1b). Rays which reflect at this angle are tangent to a caustic surface at

$$R_c \equiv R_w \frac{m}{\nu_{mp}}. \qquad (10)$$

Alternately, by substituting equation (8) to find the radius of zero radial gradient,

$$\nabla S \cdot \hat{r} = \frac{1}{k_f} \sqrt{k_r^2 - \frac{m^2}{r^2}}; \qquad r(\nabla S \cdot \hat{r} = 0) = R_c \qquad (11)$$

6

directly yields the minimum radius of the ray trajectories, that of the caustic surface. The interpretation of the caustic radius also extends to the field representation (equations (1) and (2)). For $r > R_c$, the fields are oscillatory, while for $r < R_c$, the fields are evanescent, and drop monotonically to zero at the axis.

This geometric description of ray propagation is valid in the limit where the field variation scale length is large compared to a wavelength. This is satisfied in highly overmoded waveguides far from cutoff. For the experiments discussed here, this scale length is of the order of 1.5 times the wavelength. For this reason, we use the geometric optics approximation for its simplicity in our experimental design, but take every opportunity to compare our results with diffraction predictions as a precaution.

In the geometric optics limit, we use the following model for radiation from the launcher aperture in designing the focusing mirror. The rays bounce along the inside wall of the waveguide in a polygonal helix[10], tangent to a caustic surface at R_c and propagating with an axial component given by the bounce angle

$$\theta_B \equiv \tan^{-1} \frac{k_r}{k_z}. \tag{12}$$

These rays radiate from the launcher aperture as shown in Fig. 1b. The radiation is thus limited to a range of azimuthal angles of 2α (as defined in equation (9)).

Vector Diffraction Theory

In order to calculate the radiation field of the launcher, two methods are possible: use of the wall currents as a field source, or aperture field integral methods. The latter proves to be more efficient, as the integration may be reduced to two dimensions. Since the radius defining the aperture size of the waveguide is not very large compared to the wavelength, the radiation field must be calculated by vector diffraction theory. The Stratton–Chu formula[11] is appropriate for the near field in this case. The key assumption involved is that the fields on the aperture are known exactly. The response to the Green function appropriate for radiation from a point source is integrated over all source regions, modulated by the appropriate phase and amplitude
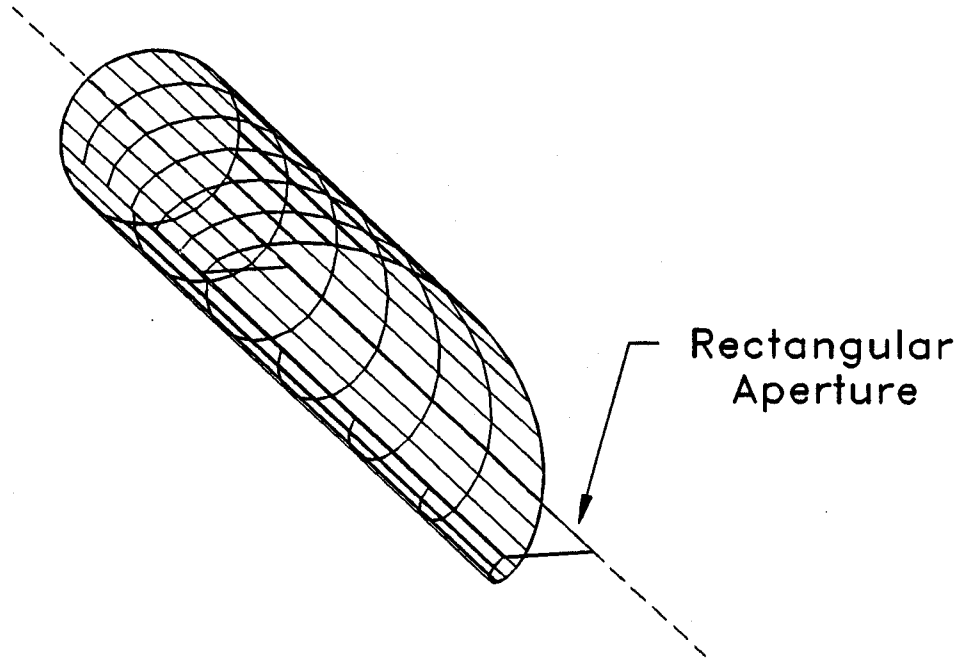
Figure 2. The helical launcher is shown in perspective, with the aperture construction used for calculation. The aperture is in the r-z plane, covering $0 \leq r \leq R_w$, and $-L/2 \leq z \leq L/2$.

for the fields in the aperture, to determine the net field at the point of observation.

The appropriate aperture is the rectangular plane bounded by the waveguide axis and the straight cut in the waveguide surface (in the axial direction), and radial boundaries at the origin and end of the helical cut (in the transverse direction), as shown in Fig. 2. The fields on this aperture are assumed to be the unperturbed waveguide fields, (equations (1) and (2)).

The field at the point of observation is given by:

$$\mathbf{E}(\mathbf{r}) = \frac{1}{4\pi} \int_{S'} \left[(\hat{n} \cdot \mathbf{E}') \nabla g_{\mathbf{r},\mathbf{r}'} + (\hat{n} \times \mathbf{E}') \times \nabla g_{\mathbf{r},\mathbf{r}'} + i\omega g_{\mathbf{r},\mathbf{r}'} (\hat{n} \times \mathbf{B}') \right] dS',$$

(13)

neglecting the contribution from source currents on the aperture boundary, where $\mathbf{E}'$ and $\mathbf{B}'$ are the fields in the aperture, $\mathbf{E}$ is the field at the observation point, and $g_{\mathbf{r},\mathbf{r}'}$ is the appropriate Green function for point

source radiation, given by

$$g_{\mathbf{r},\mathbf{r}'} \equiv \frac{e^{ik_f r}}{r} \qquad (14)$$

where k_f is the free space wavenumber, and

$$r \equiv |\mathbf{r} - \mathbf{r}'| \qquad (15)$$

is the distance from the source point to the observation point.

When calculating the fields by the above method, an additional consideration must be included. The helical cut of the launcher can shield a fraction of the rectangular aperture from some observation points. Contributions to the integrals are only included if the aperture segment is not shielded, i.e. if the line of sight between point $\mathbf{r}'$ in the aperture and the point $\mathbf{r}$ of observation does not intersect the launcher.

Unfortunately, this treatment yields a two–dimensional integral which is analytically intractable. We have written a code incorporating several numerical shortcuts to integrate the TE_{mp} waveguide mode equations in the Stratton–Chu formula over the Vlasov aperture.

The results from calculating the azimuthal dependence of the radiation pattern from the helical launcher at intermediate distances and optimum polar angle are shown in Fig. 3, compared to measurements (discussed below).

In the far–field, this treatment may be simplified to a single one–dimensional integral, which allows for faster calculation (see Appendix). The resulting E_ϕ component is also shown in Fig. 3. The far–field expansion is a good approximation to the near–field case at intermediate distances (the Fresnel zone).

Launcher

In the plane wave approximation, the helical flow of energy in the waveguide can be represented as circulating rays tangent to the caustic, as described above. It is essential that the waves are unperturbed until they are incident on this aperture, thus the waveguide opening must be cut open in a helical shape — with the helical cut following the ray trajectories in the guide.
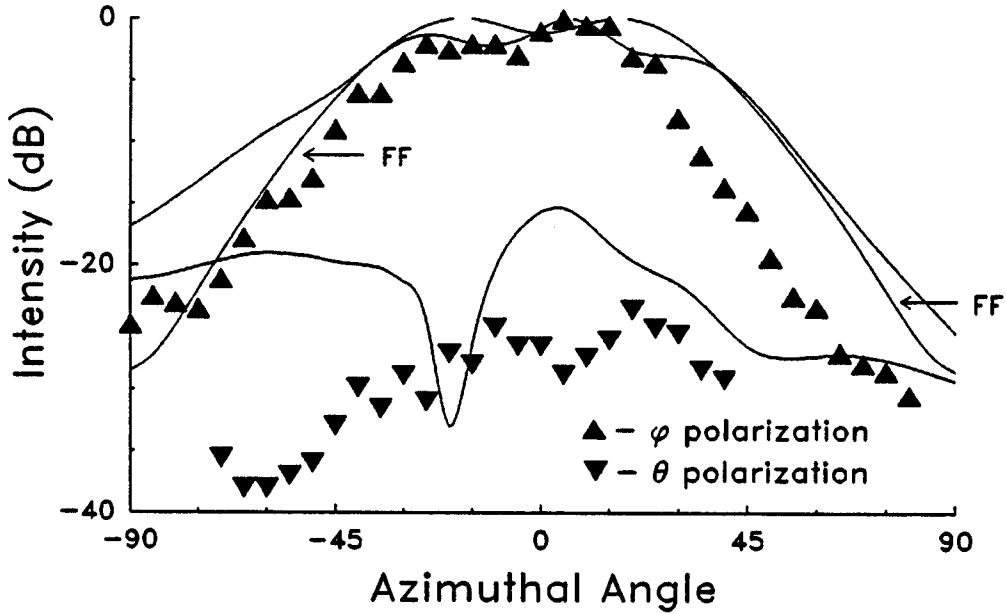
Figure 3. The E_ϕ and cross polarization components of the $TE_{16,2}$ mode radiation pattern from the launcher at the optimum polar angle of $\theta = 25.4°$ are shown, as calculated by a near–field Stratton–Chu calculation at $r = 25$ cm. The indicated line shows the far–field approximation to E_ϕ. The data points are measurements at 25 cm.

The penalty for having a launcher length that is too short is that radiation will "spill over" the helical cut of the launcher. This radiation will be randomly distributed in azimuthal angle and polarization — i.e. not recoverable in the succeeding chain of focusing mirrors. In the extreme limit, the radiation from a short launcher approaches that of a circular aperture; a hollow cone with non–uniform polarization.

In the geometric optics limit there is no penalty for too–long a launcher. A more careful examination shows, however, that the self–shielding and extended "slit" of a too long launcher will cause mode–conversion and enhanced losses[12].

Previous work[2,5,6] has assumed the correct length to be the "bounce length", the axial distance along the guide propagated by a wave bouncing at angle θ_B in traversing the guide circumference $2\pi R_w$,

$$L_B \equiv 2\pi R_w \frac{k_z}{k_r} = 2\pi R_w \sqrt{\frac{k_f^2}{k_r^2} - 1}. \tag{16}$$
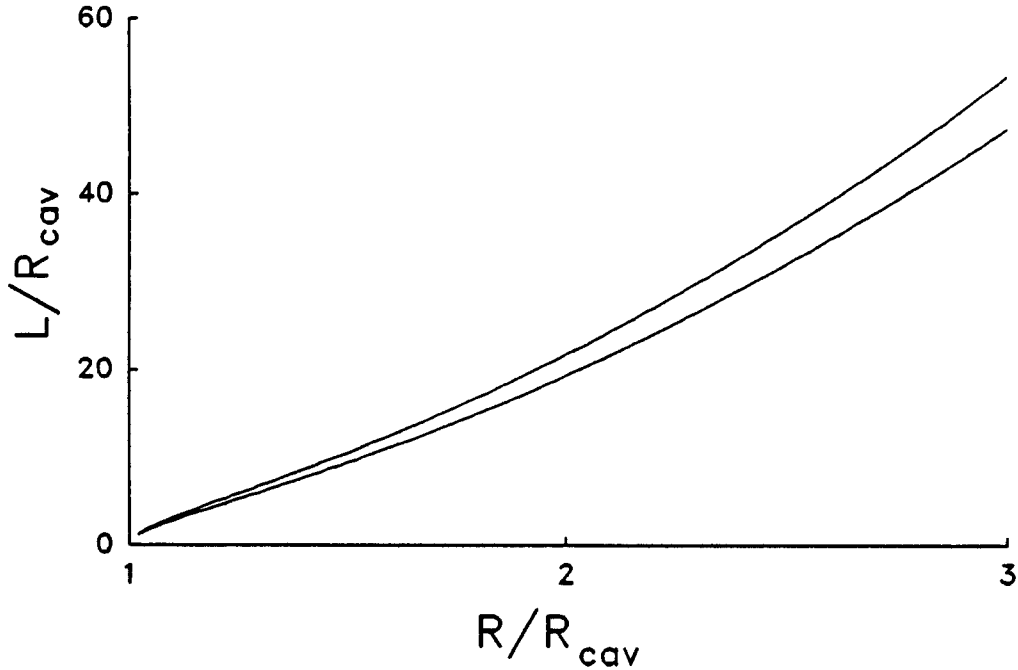
10

Figure 4. The length of the launcher increases quickly as the launcher radius increases. The upper line shows the curve for the bounce length, L_B. The lower line shows the modified length, after correcting for conservation of energy flux (at a mode number of $TE_{16,2}$).

If the wave propagating in the guide is generated near cutoff in a gyrotron cavity of radius R_{cav}, then

$$k_f \approx k_{r,cav} = \nu_{mp}/R_{cav} \qquad \text{thus} \qquad L_B \approx 2\pi R_w \sqrt{\frac{R_w^2}{R_{cav}^2} - 1}. \qquad (17)$$

Equation (17) indicates that the bounce length is independent of the mode (i.e. independent of ν_{mp}) for modes generated near cutoff in a gyrotron cavity and propagated out into an overmoded guide. If the above bounce length is the correct length for the launcher, then the launcher length would be independent of the operating mode in the gyrotron.

Fig. 4 shows how the launcher length depends on the waveguide radius. To keep the launcher reasonably short, the output waveguide radius must be as small as practical. This must be balanced against a desire to keep the wave impedance close to that of free space to minimize impedance mismatch reflections.
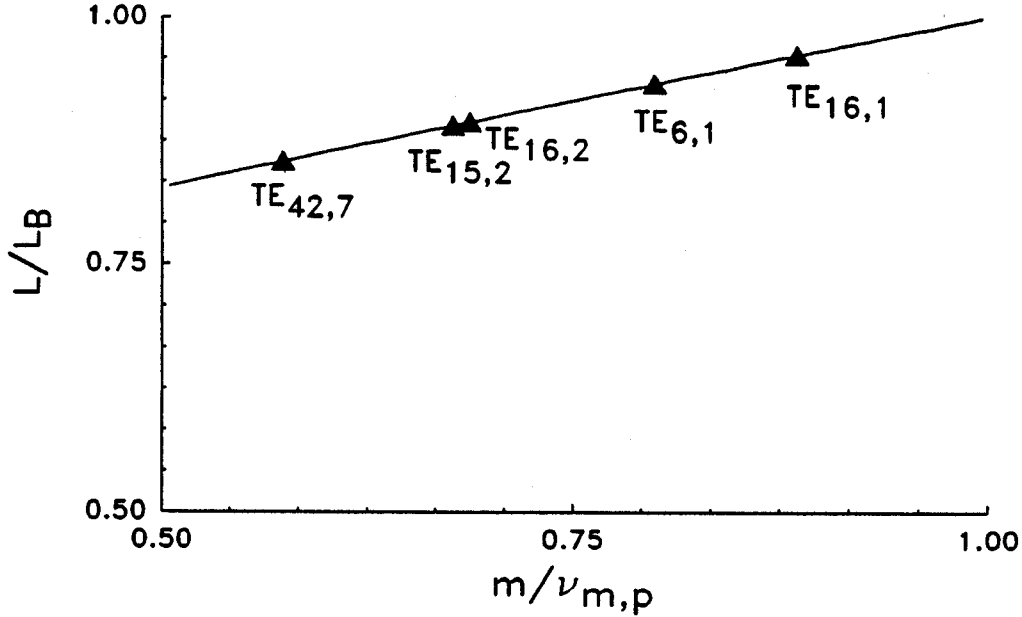
11

Figure 5. The modification factor for the conservation of energy correction to the coupler length, as a function of the ratio m/ν_{mp}. The values for a few significant mode numbers are shown.

We have calculated the length of the Vlasov launcher by integrating the normal component of the Poynting vector of a rotating waveguide mode over an aperture of height R_w and length L, the aperture shown in Fig. 2. By equating the energy flux through the waveguide cross section to that through the rectangular aperture defined above, we find the correct length L to be given by:

$$L = L_B \frac{\left(\nu_{mp}^2 - m^2\right)}{\nu_{mp}} \frac{J_m^2(\nu_{mp})}{J_m^2(\nu_{mp}) + 2\sum_{l=1}^{\infty} J_{m+l}^2(\nu_{mp})}. \tag{18}$$

Fig. 5 shows the ratio L/L_B as a function of m/ν_{mp}. For true whispering gallery modes ($m \gg 1$ and $p = 1$), m/ν_{mp} converges to 1, as does this correction factor (L/L_B).

Although the correction factor is mode number dependent, this variation is very weak over the step tuning range of a high power gyrotron, since the azimuthal and radial mode numbers tune together with the ratio m/ν_{mp} approximately constant.

12

A coupler could be cut to the length corresponding to the pitch angle of the wall currents[6]. The wall currents are seen to rotate at a stronger helical pitch angle than the radiation, as found by:

$$\text{current } \kappa \propto \mathbf{n} \times \mathbf{H} \text{ at wall,} \tag{19}$$

where $\hat{n}$ is the normal unit vector at the wall. This pitch angle corresponds to a very short launcher length,

$$L' = 2\pi R_w \frac{|H_\phi(R_w)|}{|H_z(R_w)|} = L_B \frac{m}{\nu_{mp}}. \tag{20}$$

Very low efficiency (75% for the $\text{TE}_{16,2}$ mode) should be seen with a launcher of this length, due to the losses over the helical edge.

An alternate intuitive approach[6] uses the following correction to the bounce length derivation. Since the rays do not exactly skim along the wall, equating $2\pi R_w/L$ to the tangent of the pitch angle is not correct. The effective azimuthal path length is instead determined by the sum of chords which are tangent to the caustic radius (mR_w/ν_{mp}) on each bounce. The bounce length must then be multiplied by the ratio of the chord length to arc length for one chord:

$$L'' = L_B \frac{\sin \alpha}{\alpha}, \tag{21}$$

where α is the azimuthal spread angle defined above ($\cos \alpha \equiv \frac{m}{\nu_{mp}}$). Although they are not equal, the approximation

$$L'' \approx L \tag{22}$$

can be shown numerically to be correct to within 0.1% for a wide range of mode numbers.

Design of the Reflector

The radiation from the helical launcher requires focusing and profile shaping before it is suitable for transmission as a Gaussian beam. The reflector is designed for focusing in the azimuthal direction only, as its cross–section is constant along the axial direction.

For simplicity, we use geometric optics (from the plane wave expansion and far–field expansions) to design our reflector. We then
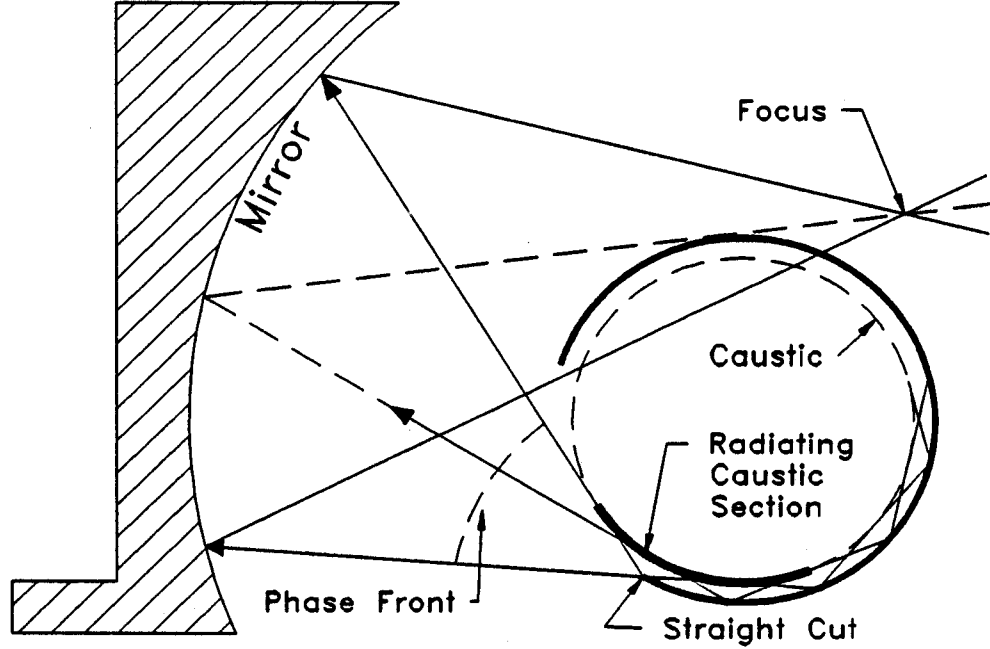
Figure 6. A cross section of the launcher and mirror geometry shows the arc of the caustic which can be treated as the radiating source, the extreme rays, an intermediate phase front, and the focus.

use the near–field calculation to check our results. A geometric optics construction of the phase front is used to design the reflector, see Fig. 6. The radiating source is assumed to be an arc segment of the caustic bordered by the extreme rays. By the plane wave expansion (equations (3) — (6)), a bundle of rays is generated to fill the aperture. The source points of these rays are considered to be the last tangency to the caustic surface before being emitted through the aperture. In addition, there is a uniform distribution of rays leaving the caustic source with a phase variation of

$$E(\phi, z) \propto e^{i(m\phi + k_z z)}. \tag{23}$$

A phase front can be constructed from rays with identical path lengths, where the paths are measured along the straight path tangent to the caustic plus the fraction of the caustic travelled from a common point. The mirror surface is designed by satisfying the constraints of 1) focusing the rays at a given point and 2) constant phase at the focus. The locations of the mirror center and the focal point can be chosen

14

arbitrarily — we select these by adding the constraint of optimizing the angular distribution of rays converging on the focus to approximate a Gaussian distribution.

The reflected rays must also not intersect the launcher *en route* to the focal point. This either constrains the reflector to a distance $r \gtrsim 3R_w$ from the launcher wall, or requires that the reflection angle be tilted to direct the beam away from the launcher. The second method leads to a better approximation of the Gaussian transverse distribution.

Hardware

Measurements were made using the rotating WGM generated by the MIT megawatt gyrotron, (typically operating at about 0.6 MW in 1 μsec pulses). The frequency was step tunable from 126 to 328 GHz, corresponding to the $TE_{12,2}$ through the $TE_{27,6}$ modes. These experiments were performed at 148.8 GHz in the $TE_{16,2}$ mode.

A sleeve was fixed to the gyrotron window and the rotatable launcher attached behind it. The window gap unfortunately created spurious modes which could be observed by far field scans. Careful alignment of the mounting sleeve was necessary to minimize this effect. Ultimately, better than 90% mode purity was achieved (with most of the impurity in the $TE_{16,1}$ mode). Operation without the sleeve showed no measurable $TE_{16,1}$ impurity, and confirmed that the spurious mode generation was due to the window gap. In addition, the azimuthal scans of the launcher far field were performed with the detector centered on the main polar lobe of the radiation. Azimuthal scans were done by rotating the launcher on the sleeve. The reflector was mounted on an independent platform, with 1 mm alignment tolerances.

Intermediate field measurements (launcher azimuthal scans) were made with a Hughes WR6 diode detector with a WR6 21 dB pyramidal horn. Short distance measurements (launcher edge scans, and mirror focus scans) were made with a truncated WR6 waveguide receiver rather than a horn, for spatial localization and less directivity.

Calorimetric measurements were made with a Scientech model 362 laser calorimeter with a 36–0401 head modified for a 12.5 cm diameter absorbing plate with 95% absorption at 140 GHz. Detailed

calibration measurements of the calorimeter surface have shown the absorption coefficient to be fairly independent of the angle of incidence. The gyrotron was pulsed at 6 Hz, and efficiencies were measured by normalizing to power measurements taken with the launcher removed.

The nominal gyrotron power was measured by placing the calorimeter several cm from the end of the circular waveguide. The mirror efficiency measurements were made by placing the calorimeter at the linear focus from the reflector. Since the focal line is longer than the width of the calorimeter, a square eccosorb mask was placed over the calorimeter, and the measurement was done in three segments to cover the width of the line. Relative uncertainty in the lateral alignment of the segments was about 2 mm, giving an uncertainty in the power measurement due to misalignment (overlap or gap) of the segments of about $\pm 2\%$.

Experimental Results

The field distribution of the aperture (see Fig. 2) was measured along the axial cut of the launcher, at several radial positions, see Fig. 7. Clearly the conventional bounce length, L_B, is too long — the signal is characteristically 25–30 dB down at this position. Similarly, the wall current length, L' is clearly too short, as about 15% of the power is radiated beyond this point.

We conjecture that there is a failure in the assumption of unperturbed waveguide fields between L' and L. This is due to the difference in pitch angle between the average energy flux in the waveguide and the wall currents. At $z < L'$, the wall currents and radiation energy flux in the launcher are effectively unperturbed by the launcher, i.e. the respective pitch angles trace backwards smoothly into the waveguide. At $z > L'$, this is not true, as the steeper pitch angle of the wall currents traces back to a region perturbed by the launcher aperture. This also implies that a launcher of length L' might generate the "cleanest" radiation pattern, in spite of the inherent low efficiency.

An azimuthal scan of the radiation pattern from the launcher at the polar angle of peak radiation is shown in Fig. 3. The data points show a scan of the E_ϕ component of the $TE_{16,2}$ mode, while the solid lines show the theoretically predicted results. The reasonable agreement between theory and experiment indicates that the assumptions
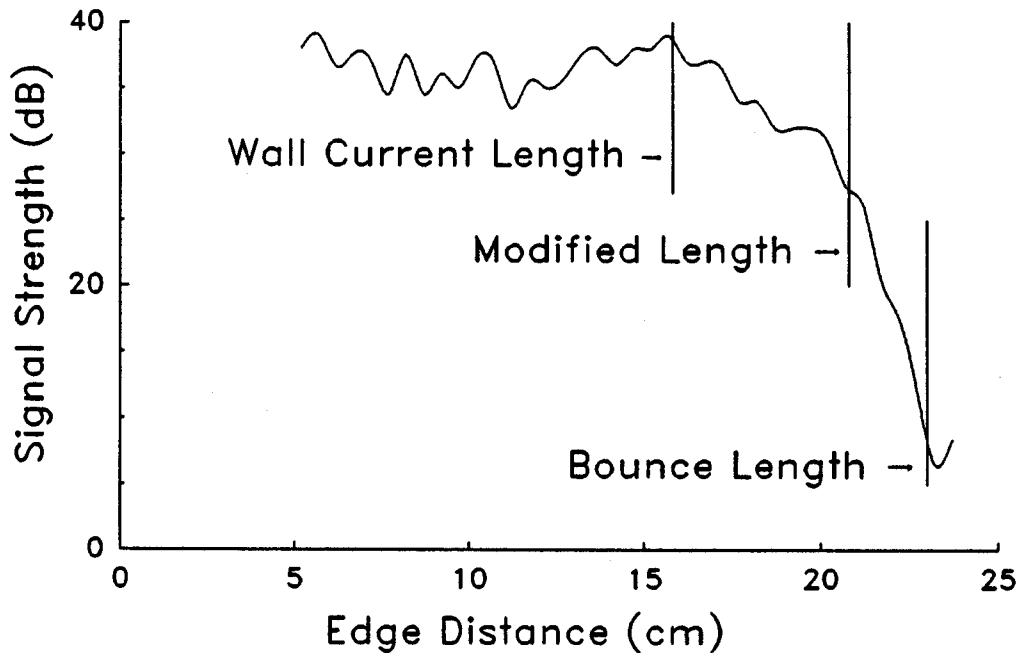
Figure 7. The measured radiation intensity is shown as measured along the length of the straight edge of a launcher of length about L_B. Measurements were made with a receiving antenna constructed of truncated WR6 waveguide, scanned 0.2 cm from the waveguide wall in an $r = 1.74$ cm launcher radiating $TE_{16,2}$ at 148.8 GHz. (Fluctuations with axial distance were often larger than above on similar scans, presumably due to the steep gradients in field strength and uncertainty in alignment of the receiver relative to the radiating edge. The characteristic signal strength vs. axial distance is very reproducible.)

connected with the aperture field method are valid. The cross polarization (E_θ) component does not show the same quality of agreement, although the predicted 20–25 dB drop compared with E_ϕ is reasonably accurate.

Fig. 8 shows measurements made on a vertical scan through the line focus in the focal plane at two different locations (using a diode receiver and a truncated WR6 waveguide as a receiving antenna). The power is seen here to be well focused, with a FWHM of 5.5 mm, or 2.25 λ.

Calorimetry measurements were made with the reflector, and launchers of three different lengths (and corresponding helical pitches). The short launcher was cut to the wall current length, L'; the medium
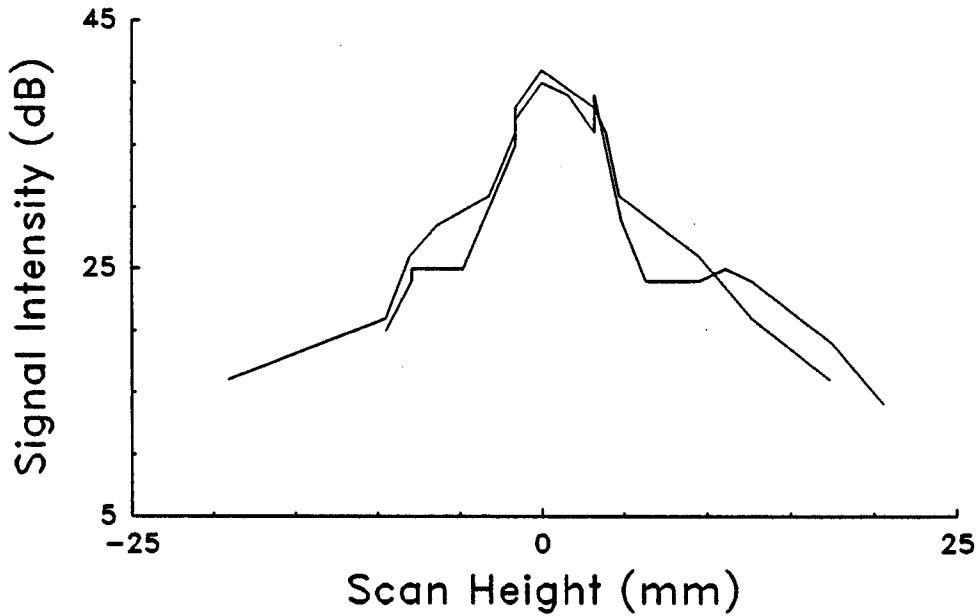
Figure 8. The measured radiation intensity of the E_ϕ polarization measured at the focus line after reflection off the mirror is shown at two axial distances 12.0 cm apart. The receiving antenna is a truncated WR6 waveguide, for spatial localization.

cut to L; and the long launcher cut slightly short of the bounce length, L_B. The following table shows these results.

LENGTH	EFFICIENCY
$L' = 15.8$ cm	69.0%
$L = 20.4$ cm$(\approx L'')$	91.4%
$\lesssim L_B = 21.9$ cm	85.6%

The correct length L shows the highest efficiency, 91.4%, further confirming this as the appropriate length.

Efficiency Estimates

The efficiency of the mode converter can be estimated numerically, using the near–field calculation, and the radiation azimuthal angle range subtended by the first mirror. Fig. 9 shows the azimuthal angle dependence of the radiation pattern at optimum polar angle, at a 9 cm distance from the center of the aperture (as aligned in the experiment).
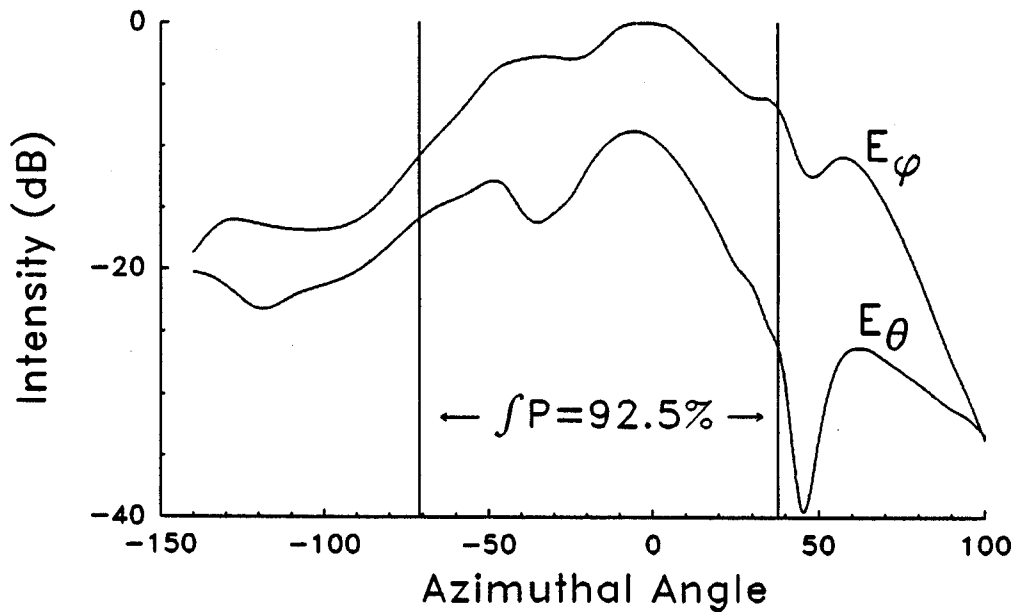
Figure 9. The E_ϕ and E_θ polarization components of the near–field radiation pattern are calculated at $s = 9$ cm, (the mirror distance). Numerically integrating the power in this pattern gives a relative efficiency of 92.5% between the azimuthal angles subtended by the mirror.

The power is integrated within the angle limits of the first mirror, with a predicted 92.5% total efficiency (i.e. both polarizations), as compared to the measured value of 91.4%. Note that the majority of the missing power is at larger values of ϕ, which corresponds to rays tangent at a radius smaller than the caustic radius — a "soft" boundary.

The penalty for a too–short coupler is the loss of radiation over the backside of the helical coupler, as discussed above. Using this idea, the relative efficiency loss for the 15.8 cm coupler can be estimated from the ratios of the lengths — the short launcher should show 77% of the efficiency of the conservation of energy length, or 77%×91%=70%. This is compared with the measured efficiency of 69%.

Summary

We have shown a new method for determining the proper length of a helical Vlasov launcher for mode conversion of rotating whispering gallery modes to low mode number linearly polarized radiation, which leads to optimum efficiency. We have also designed an optimized reflector for the mode conversion system. Both launcher and reflector

were tested experimentally and achieved 91.4% efficiency, in agreement with theory. A robust numerical code has been developed for calculating near–field radiation patterns from the launcher, which agrees well with experimental measurements.

ACKNOWLEDGEMENTS

APPENDIX: Far Field Approximation

Although far–field approximations are not particularly relevant for the launcher to mirror distances used in this experiment, the asymptotic form of the radiation pattern in the far–field gives valuable insight towards understanding the detailed radiation pattern.

Derivation of the far field equation uses the Franz formula[11], (an equivalent form of the Stratton Chu formula, in which only the field components in the plane of the aperture contribute to the radiation fields), which is integrated over the rectangular aperture, as before:

$$\mathbf{E(r)} = \frac{1}{4\pi}\nabla \times \int \hat{n} \times \mathbf{E}' g_{\mathbf{r},\mathbf{r}'} \, d\mathbf{S}' + \frac{ic^2}{4\pi\omega}\nabla \times \nabla \times \int \hat{n} \times \mathbf{B}' g_{\mathbf{r},\mathbf{r}'} \, d\mathbf{S}'. \quad (24)$$

In the far field approximation, $r \equiv |\mathbf{r} - \mathbf{r}'|$ can be approximated in the Green function by:

$$g_{\mathbf{r},\mathbf{r}'} \equiv \frac{e^{ik_f r}}{r} \approx \frac{e^{i(k_f r - \mathbf{k}_f \cdot \mathbf{r}')}}{|\mathbf{r}|}. \quad (25)$$

To evaluate equation (24) for the fields defined by (1) and (2), a transformation must be made from the cylindrical (waveguide) coordinate system to rectangular coordinates to perform the integral. A further transformation to spherical coordinates is preferable for interpretation of the result. The cylindrical to spherical transformation

20

preserves the azimuthal angle (ϕ), while the polar angle (θ) is defined as the elevation from the $+\hat{z}$ axis. The aperture is defined to be in the $\phi = -\pi/2$ plane. The del operator can be taken as ik_f for large distances. The integral over the length of the aperture can be solved analytically, yielding (in the far field limit):

$$
\mathbf{E} = Z_0 H_0 \frac{k_f}{4\pi} \frac{e^{ik_f r}}{r} f_0(\theta) \frac{i}{k_r} \Big[
$$

$$
\left(\frac{ik_z}{k_r} \sin\theta f_2(\theta,\phi) - \cos\theta \sin\phi f_3(\theta,\phi) \right) \hat{\theta} , \quad (26)
$$

$$
- \left(\cos\phi f_3(\theta,\phi) + \frac{mk_f}{k_r} \sin\theta f_1(\theta,\phi) \right) \hat{\phi} \Big]
$$

where

$$
f_0(\theta) \equiv L \, \frac{\sin\left(\frac{k_f L}{2}(\cos\theta - \frac{k_z}{k_f}) \right)}{\frac{k_f L}{2}(\cos\theta - \frac{k_z}{k_f})} , \qquad \text{and} \qquad (27)
$$

$$
f_1(\theta,\phi) = \int_0^{\nu_{mp}} d\nu \frac{J_m(\nu)}{\nu} e^{i\frac{k_f}{k_r}\nu \sin\theta \sin\phi} ,
$$

$$
f_2(\theta,\phi) = \int_0^{\nu_{mp}} d\nu J_m'(\nu) e^{i\frac{k_f}{k_r}\nu \sin\theta \sin\phi} , \qquad (28)
$$

$$
f_3(\theta,\phi) = \int_0^{\nu_{mp}} d\nu J_m(\nu) e^{i\frac{k_f}{k_r}\nu \sin\theta \sin\phi} .
$$

The three integrals are shown in Fig. 10. From equation (27), it can be seen that the far–field radiation pattern is quite peaked at $\theta = \theta_B$, and that equations (28) act as slowly varying envelopes around the fast $f_0(\theta)$ modulation. Furthermore, it can be shown numerically from (26) and (28) that the E_ϕ term dominates. The plane wave interpretation of the resulting pattern is that the radiation is azimuthally polarized, directed at $\theta = \theta_B$, and has an azimuthal distribution given by equation (26).
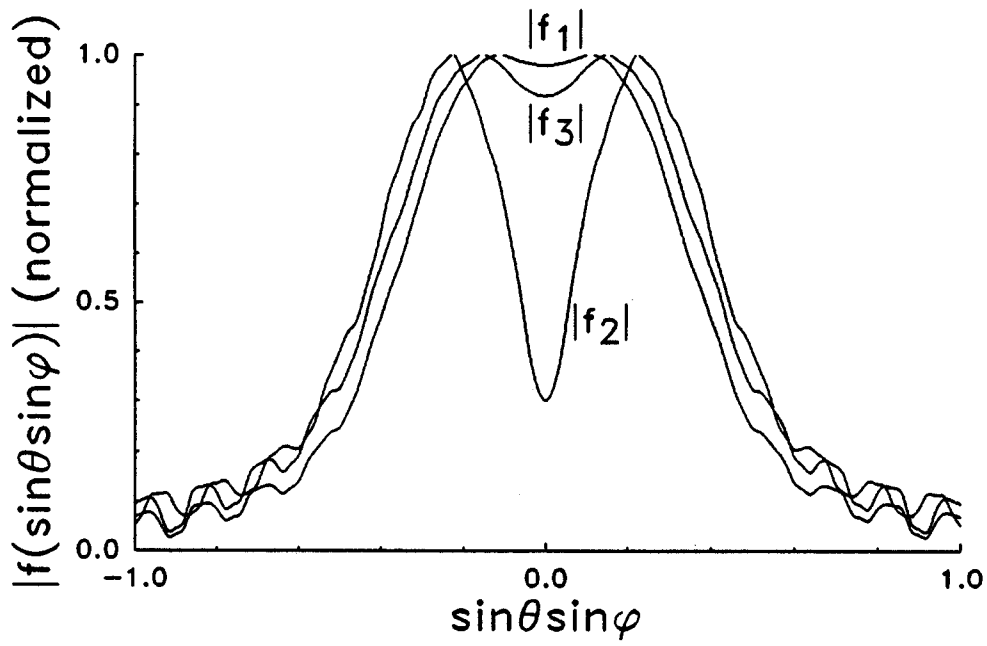
Figure 10.   The three envelope integrals in the far–field expansion
of the Franz formula are shown as a function of spatial angle (for the
$TE_{16,2}$ mode with $k_f/k_r = 2$). All three functions are slowly varying,
compared to the rapid modulation in θ of $f_0(\theta)$.

References

*Present Address: Kernforschungszenstrum Karlsruhe, Institut für Technische Physik, Karlsruhe, W. Germany.

[1] C. Dragone, IEEE Trans. Microwave Theory and Techniques, **MTT–28**, 704 (1980).

[2] S.N. Vlasov, L.I. Zagryadskaya, and M.I. Petelin, Radio Eng, **20**, 14, (1975).

[3] M.J. Buckley, G.H. Luo, R.J. Vernon. *Thirteenth International Conference on Infrared and Millimeter Waves*, Richard J. Temkin, Editor, SPIE **1039**, p117 (1988).

[4] M. Thumm, L. Rebuffi, H.J. Barkley, A. Jacobs, G.A. Müller. *Thirteenth International Conference on Infrared and Millimeter Waves*, Richard J. Temkin, Editor, SPIE **1039**, p463 (1988).

[5] B.G. Danly, K.E. Kreischer, W.J. Mulligan, and R.J. Temkin. IEEE Trans. Plasma Sci. **PS–13** pp383 (1985).

[6] O. Wada, M. Hashimoto, and M. Nakajima. Int. J. Elect. **65** pp725 (1988).

[7] K.E. Kreischer, T.L. Grimm, W.C. Guss, A.W. Möbius, R.J. Temkin. "Experimental Study of a High Frequency Megawatt Gyrotron Oscillator", Phys. Fluids **2**, 640 (1990).

[8] M.K. Haldar, A.H. Beck, Electronics Letters, **15**, (1979).

[9] The following equivalence is useful:

$$\frac{m}{x} J_m(x) = \frac{1}{2\pi} \int_0^{2\pi} d\phi' \, \cos \phi' e^{i(x \sin \phi' - m\phi')}.$$

[10] L. A. Weinstein, "Open Waveguides and Open Resonators", pp 139, Golem Press, Boulder, Colorado (1969).

[11] Jin Au Kong, "Electromagnetic Wave Theory", pp 381, John Wiley & Sons, (1986).

[12]A long launcher will appear like a superposition of the proper aperture and an axial slit in the waveguide preceding the aperture. Such a slit will interrupt wall currents, causing mode conversion. The most likely mode conversion in such a case will be to the opposite rotating mode (thus giving a null in the wall currents on the slit). Any power converted to the opposite rotation will "spill" over the helical cut of the launcher, thus reducing efficiency.